Received: 23 July 2020 | Revised: 8 December 2020 | Accepted: 9 December 2020

DOI: 10.1111/joa.13389

ORIGINAL PAPER

Journal of Anatomy ANATOMICAL SOCIETY WILEY

Low elbow mobility indicates unique forelimb posture and function in a giant extinct marsupial

Hazel L. Richards[1,2] | Peter J. Bishop[3,4] | David P. Hocking[1,2] | Justin W. Adams[5] | Alistair R. Evans[1,2]

[1]School of Biological Sciences, Monash University, Clayton, Vic, Australia

[2]Geosciences, Museums Victoria, Melbourne, Vic, Australia

[3]Structure and Motion Laboratory, Department of Comparative Biomedical Sciences, Royal Veterinary College, Hatfield, UK

[4]Geosciences Program, Queensland Museum, Brisbane, Qld, Australia

[5]Department of Anatomy & Developmental Biology, School of Biomedical Sciences, Faculty of Medicine, Nursing and Health Sciences, Monash University, Clayton, Vic, Australia

Correspondence
Hazel L. Richards, School of Biological Sciences, Monash University, Clayton, Vic., Australia.
Email: hazel.l.richards@gmail.com

Funding information
This research was supported by an Australian Government Research Training Program Scholarship and Monash University-Museums Victoria PhD Research Scholarship (HLR), internal funds from the Department of Anatomy and Developmental Biology, Monash University (JWA), and the Australian Research Council DP180101797 (ARE).

Abstract

Joint mobility is a key factor in determining the functional capacity of tetrapod limbs, and is important in palaeobiological reconstructions of extinct animals. Recent advances have been made in quantifying osteological joint mobility using virtual computational methods; however, these approaches generally focus on the proximal limb joints and have seldom been applied to fossil mammals. *Palorchestes azael* is an enigmatic, extinct ~1000 kg marsupial with no close living relatives, whose functional ecology within Australian Pleistocene environments is poorly understood. Most intriguing is its flattened elbow morphology, which has long been assumed to indicate very low mobility at this important joint. Here, we tested elbow mobility via virtual range of motion (ROM) mapping and helical axis analysis, to quantitatively explore the limits of *Palorchestes*' elbow movement and compare this with their living and extinct relatives, as well as extant mammals that may represent functional analogues. We find that *Palorchestes* had the lowest elbow mobility among mammals sampled, even when afforded joint translations in addition to rotational degrees of freedom. This indicates that *Palorchestes* was limited to crouched forelimb postures, something highly unusual for mammals of this size. Coupled flexion and abduction created a skewed primary axis of movement at the elbow, suggesting an abducted forelimb posture and humeral rotation gait that is not found among marsupials and unlike that seen in any large mammals alive today. This work introduces new quantitative methods and demonstrates the utility of comparative ROM mapping approaches, highlighting that *Palorchestes*' forelimb function was unlike its contemporaneous relatives and appears to lack clear functional analogues among living mammals.

KEYWORDS
biomechanics, forelimb, functional morphology, helical axes, joint mobility, megafauna, *Palorchestes*, range of motion

Abbreviations: ABAD, abduction-adduction; AMNH, American Museum of Natural History; DOF, degree of freedom; FE, flexionextension; JCS, joint coordinate system; LAR, long-axis (axial) rotation; MU, Monash University collection; NMV C, Museums Victoria Mammalogy collection; NMV P, Museums Victoria Palaeontology collection; QVM, Queen Victoria Museum; ROM, range of motion; SAMA P, South Australian Museum palaeontology collection; WCS, world coordinate system.

1 | INTRODUCTION

Posture and limb function are fundamental aspects of reconstructing the palaeobiology of extinct animals, and our estimations of these can be constrained via range of motion (ROM) analyses of key joints. Recently, considerable progress has been made toward repeatable, quantitative assessment of osteological joint mobility in fossil animals using virtual methods informed by modern analogues. Much of this work has focused on extant diapsid hip joints as models for archosaur posture and locomotion (e.g., Brassey et al., 2017; Mallison, 2010; Manafzadeh & Padian, 2018), or on extant sprawling animals to understand early evolution of the tetrapod limb (Lai et al., 2018; Nyakatura et al., 2015; Nyakatura et al., 2019; Pierce et al., 2012; Regnault & Pierce, 2018). Few modern studies have examined mammals, and these techniques have not yet been applied to marsupials. Additionally, studies of extant species have almost ubiquitously focused on the proximal-most joints of the limb (i.e. hip or shoulder). Although palaeontological studies have sometimes investigated more distal limb joints (e.g. Carpenter & Wilson, 2008; Lai et al., 2018; Senter & Robins, 2005), these are not typically directly validated against modern species (but see Pierce et al., 2012). The potential complexity of joint form-function relationships in more distal joints therefore remains to be comprehensively explored in a quantitative way.

One application of these new approaches is in delimiting the functional capabilities of extinct animals bearing extreme or unusual morphology. *Palorchestes azael* Owen, 1873 (Diprotodontia: Vombatiformes) exemplifies this as an extinct giant marsupial known for its strange skull with purported 'trunk' and highly unusual, flattened elbow joint morphology (Mackness, 2008). *Palorchestes* was a rare and enigmatic member of Australia's extinct Pleistocene marsupial megafauna, whose closest surviving relatives are the wombats and koala (Black et al., 2012). Appearing in the fossil record from at least 270 ka to approximately 40 ka (Roberts et al., 2001; Shean, 2007), it expressed a suite of morphologies that seem to indicate a specialised browsing habit (Coombs, 1983)—a tapered elongate snout with retracted nasals, enormous but mediolaterally narrow recurved claws, and highly robust forelimbs (Richards et al., 2019). Additionally, the remarkably flat shapes of the trochlear articulation between its humerus and ulna suggest that the elbow in *Palorchestes* had very limited mobility in the parasagittal plane. While the peculiarity of its elbow has long been recognised (Flannery & Archer, 1985), the functional capacity of the *Palorchestes* forelimb has never been examined.

In contrast to the highly mobile humeroradial joint (e.g. Bonnan et al., 2016), the mammalian humeroulnar joint is generally treated as a single degree of freedom (DOF) 'hinge' joint with flexion-extension as the sole axis of rotation (Fujiwara, 2009; Haines, 1946). However, recent studies have suggested that in some cases the humeroulnar articulation can be considered a multiaxial joint. In some mammals, the rotations at the humeroulnar joint have been measured in three degrees of freedom; flexion-extension, as well as long-axis rotation and abduction-adduction (Fujiwara & Hutchinson, 2012). This is often termed 'joint laxity' when explored in human studies (Bottlang et al., 2000). The flattened elbow seen in *Palorchestes* suggests that simple hinge-like flexion-extension movement was restricted, but this joint may have allowed more complex movements involving multiple DOFs simultaneously.

Traditionally, ROM is measured as minimal and maximal rotations of a joint from a reference pose, where rotational axes are assigned to anatomical movements, and rotation about each axis is measured with the remaining axes held constant in a zero position. A major shortcoming of this 'one-at-a-time' approach is that it does not capture interactions between rotations (e.g., flexion may be restricted in a maximally abducted joint), or 'off axis' movements, both of which might occur in the unusual elbow joint of *Palorchestes*. The three-dimensional joint ROM mapping approach established by Haering et al. (2014) and further developed by Kambic et al. (2017) and Manafzadeh and Padian (2018) provides a way to explore and visualise the true maximum ROM of the *Palorchestes* elbow and compare this with other mammals. By assigning the same coordinate system to each taxon and freely manipulating virtual models of their elbow joints across three DOFs simultaneously, each pose (a unique combination of three sequential Euler rotations) can be plotted as a three-dimensional (3D) coordinate to visualise 'envelopes' of possible movements. These envelopes characterise interactions among joint rotations, and provide a more realistic idea of *in vivo* joint kinematics than separate uniaxial rotations (Kambic et al., 2017). The ROM envelopes generated for each taxon can then be superimposed into a shared angle—angle—angle space, where we can quantify and interpret differences in their relative position, extent, and shape as a way of comparing elbow functional capacity.

In addition to rotations, some joints may also be capable of undergoing translations not captured via 3 DOF analyses. Complex movement incorporating both rotation and translation (i.e., 6 DOFs) can be addressed by quantifying finite and instantaneous helical axes (Figure 1). The 3D movement of the ulna relative to the humerus, from one disposition in space to another, can be described by a rotation of the ulna around an axis, and simultaneous translation along that same axis – that is, a helical motion (Ehrig & Heller, 2019). Rotations about and translations along each of the three Cartesian axes of a joint coordinate system can therefore be more concisely expressed as a rotation about and translation along a single axis, the details of which are derived using linear algebra (e.g., Spoor & Veldpaus, 1980). It is important to recognise that this helical axis is usually oriented askew relative to the axes of the joint coordinate system and their constituent bones. The continuous movement from a maximally flexed to a maximally extended elbow pose can be addressed using a finite number of intermediary poses, and the helical axis determined for the transformations between each successive pose, forming a discrete approximation of instantaneous helical axis movement. By accounting for rotations and translations in all 6 DOFs, helical axes help identify the overall or 'average' axis of rotation for a given joint, that is, the axis about which rotational motion is greatest. Thus, computation of

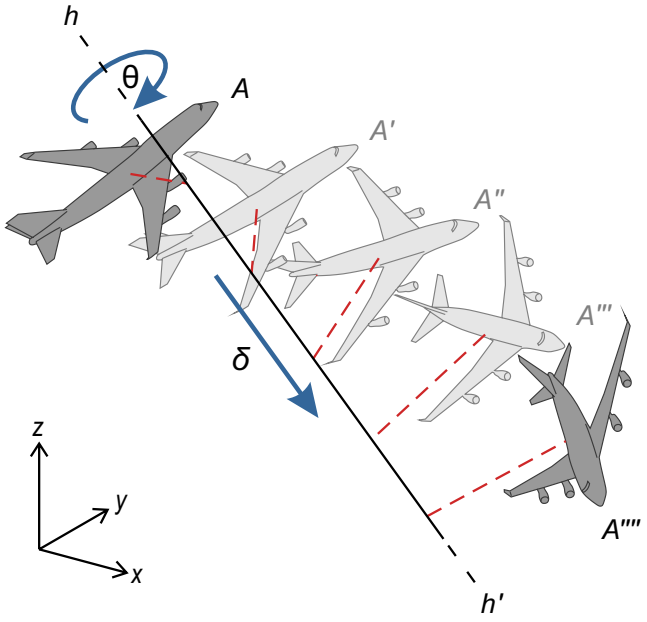

FIGURE 1 Describing motion using helical axes. Any affine transformation of an object from one attitude (position and orientation) to another can be represented as a translation δ along an axis coupled with a rotation θ about that same axis. Thus the transformation of the aeroplane A → A′′′′ can be represented as a finite helical transformation along and about a single axis hh′, which need not be parallel to any of the coordinate system axes (x, y, z). However, if detail was known about the intermediate attitudes of the aeroplane (A′, A″ and A‴), and these did not follow the same helical transformation as A → A′′′′, then each transformation of A → A′, A′ → A″, A″ → A‴ and A‴ → A′′′′ is potentially described by a different helical transformation. Taking subdivisions of A → A′′′′ ad infinitum, the instantaneous helical transformations will therefore continuously vary, in terms of helical axis location and orientation, as well as the amount of rotation about the axis per unit translation along the axis

a set of finite helical axes facilitates visualisation of changes in instantaneous helical axis orientation across a joint's ROM, as well as the quantitative derivation of a 'mean' helical axis, taken as a surrogate of the primary axis of motion. The latter approach has been extensively used in human biomechanics (e.g., Besier et al., 2003; Chèze et al., 1998; Stokdijk et al., 1999; Woltring et al., 1985), but has only recently been applied to the elbow of non-human species (e.g., horses; Kaashoek et al., 2019; sheep; Poncery et al., 2019). Helical humeroulnar motion has also been inferred in some Mesozoic mammals, but is thought to have become reduced in more recent clades (Jenkins, 1973).

In this study, we apply a 3D ROM mapping approach, along with a novel application of helical axis analysis exploring translational effects, to quantitatively test longstanding assumptions of low elbow mobility in *Palorchestes*. In exploring the relationship between joint morphology and mobility, we aim to constrain estimated forelimb postures and make inferences about locomotion in this animal. In addition, we map the elbow mobility of a range of extant and extinct mammals to compare ROM among potential functional analogues for *Palorchestes*. This study, the first to apply quantitative ROM mapping in a broad comparative fashion, will help provide new insight into how body size and habitual limb use may relate to elbow mobility, shedding light on the functional and ecological consequences of the unique forelimb anatomy of *Palorchestes*.

2 | MATERIALS AND METHODS

2.1 | Comparative sample

As the locomotor ecology of *Palorchestes* is unknown, we compared it to taxa with morphologically similar forelimbs and an unreduced clawed manus as seen in *Palorchestes*. However, no living species with this forelimb structure approaches the body size of *Palorchestes*, and the effect of body size on maximal osteological ROM is unknown—though *in vivo* limb ROM during a stride generally becomes more restricted in larger mammals (Biewener, 1983). To explore this, we studied comparative taxa of various body sizes, including the following species: the koala *Phascolarctos cinereus* and common wombat *Vombatus ursinus* as extant phylogenetic bracket taxa (Black et al., 2012; Witmer, 1995); similarly-sized extinct vombatiform marsupials *Zygomaturus trilobus* and *Phascolonus gigas*; and extant mammals with robust forelimb morphology that may represent functional analogues for *Palorchestes*, including the giant pangolin *Smutsia gigantea*, aardvark *Orycteropus afer*, giant anteater *Myrmecophaga tridactyla* and sloth bear *Melursus ursinus* (Table 1).

Due to logistical constraints and specimen availability, one individual of each species was analysed. For extant animals, associated bones from the left side were used. Due to scarcity of complete material for extinct species, in some cases associated elements from the same individual were mirrored (*Palorchestes* and *Zygomaturus* right radius and ulna mirrored to fit left humerus, *Phascolonus* had associated left side elements). For brevity, all taxa are referred to by genus. 3D morphology was captured either via computed tomographic scanning (Siemens Somatom go.UP, peak tube voltage 110 kV, current 63 mA, Sn filter, 0.36 mm reconstructed voxel size), with models generated in Avizo (Thermo Fisher Scientific, USA), or via structured blue light surface scanning (Artec Space Spider, mesh fusion size 0.2 mm), with models generated in Artec Studio 12 (Artec 3D, Luxembourg).

2.2 | Articulation

Our primary interest was in the humeroulnar joint, as this exhibits unusual morphology in *Palorchestes*, so we did not simulate radioulnar (pronation/supination) movements. However, we recognise that the radius will potentially restrict movements of the humeroulnar joint and so included it as a passive component of our models. The forearm was modelled as a single rigid body (Willing et al., 2014), with the radius position fixed relative to the ulna and inheriting its rotations around a single shared joint centre.

TABLE 1 Specimens used in this study, with body mass values and references for forelimb anatomy. All specimens were associated skeletons, though some fossils required mirroring for articulation (see text)

Species	Specimen	Body mass estimate (kg)	Forelimb anatomy
Palorchestes azael[a]	NMV P159792	921[b]	Richards et al., 2019
Phascolarctos cinereus	NMV C22285 (bones) MUPC2 (joint CT)	8[c]	Grand & Barboza, 2001
Vombatus ursinus	NMV C6697	36[c]	Scott & Richardson, 1988
Zygomaturus trilobus[a]	QVM 1992 GFV4, GFV246	577[b]	Scott, 1915
Phascolonus gigas[a]	SAMA P5027, P5030, P5031	738[b]	Stirling, 1913
Myrmecophaga tridactyla	AMNH 80016	33[d]	McDonald et al., 2008
Smutsia gigantea	AMNH 53846	40[b]	Steyn et al., 2018
Orycteropus afer	AMNH 51374	64[b]	Thewissen & Badoux, 1986
Melursus ursinus	AMNH 22896	105[b]	Puttaraju, 2015

[a]Extinct species.

[b]Mass estimated from minimum humeral circumferences using equations in Richards et al., 2019, PPE 27.5%.

[c]Cadaveric mass.

[d]Mean species mass (see supplementary material section 1.3).

As we were measuring a single isolated joint complex, for simplicity the humeroulnar joint coordinate system (JCS) was set up to match the world coordinate system (WCS) in Blender v. 2.79 (Blender Online Community, 2019). To do this, the humerus was aligned to the WCS by first visually fitting spheres to the capitulum and trochlea (i.e. the 'geometric method'; Hutchinson et al., 2005; Regnault & Pierce, 2018). The humerus mesh was then 'parented' to these spheres, and the midpoint between them translated to the (0, 0, 0) location in the WCS, with the sphere centroids aligned on the world Z axis. This brought the condyles of the distal humerus into alignment with the world Z axis, established the Z axis of the joint coordinate system (JCS), and placed the joint centre at the midpoint of the distal humeral articulations. Then, in lateral view, the humerus was manually aligned such that the world X axis passed through the centre of its midshaft, as judged by eye. This established the X axis of the JCS, and the resultant Y axis, orthogonal to these, passed through the sagittal plane of the humerus (Supplementary Material 1.1-1.2).

We then articulated the left ulna with the humerus in a 'neutral flexed' pose, with the ulnar shaft visually aligned to this JCS Y axis, i.e. flexed at 90 degrees to the humeral shaft. The articular distance between humerus and ulna at the joint centre of each species was set according to the joint spacing calculated from body size estimates. When establishing this initial articulation, we rotated the ulna around its long axis so that articulation with the humerus was achieved with minimal intersection of meshes (Figure S1.2.2). For some species, this 'neutral flexed' pose was not viable in that the ulna intersected the humerus, however it represented a repeatable coordinate system from which to measure subsequent rotations (Kambic et al., 2014).

The left radius was then articulated with the ulna with the dorsal surface of the radius facing anterolaterally, approximating a 'thumb-up', mid-supinated position. The proximodistal position of the radius was determined by the humeroradial joint spacing, measured from the anterior surface of the capitulum to the midpoint of the capitular fossa on the radial head (Figure S1.2.3).

Finally, a Blender animation 'empty' (a Blender object that facilitates animation) was created at the joint centre (location 0, 0, 0), with rotation axes set to match the WCS. This joint centre empty was then rotated around the Z axis to 0°, 0°, 90°, bringing its X axis into alignment with the long axis of the ulnar shaft (Figure S1.2.4). In this 'neutral flexed' pose, all objects were then arranged into a kinematic hierarchy, where the radius was parented to the ulna, and the ulna and its subordinate radius to the joint centre empty. This empty was then rotated back to 0°, 0°, 0°, bringing the ulna and radius into the reference pose from which to begin elbow ROM measurements (Figure S1.1). The local rotations of this joint centre empty formed the elbow JCS for the rig, using the Z-Y'-X" Euler intrinsic convention (the "XYZ Euler" rotation mode option in Blender, identical to the convention used by previous studies; Bishop et al., 2020; Brainerd et al., 2010; Grood & Suntay, 1983; Kambic et al., 2017; Manafzadeh & Padian, 2018). These rotations followed the right-hand rule, where FE was assigned to the Z axis (i.e. that with the most expected rotation) with positive rotations being extension, ABAD assigned to the Y' axis with positive rotations being adduction, and LAR assigned to the X" axis (i.e. that with the least expected rotation), with positive rotations being medial/internal rotation.

2.3 | Measuring multiaxial ROM

Multiaxial elbow ROM was sampled by rotating the joint centre empty (and its subordinate forearm meshes) around all three rotational DOF until mesh collision, as detected by eye. At each viable pose an animation keyframe was inserted capturing the constituent X"Y'Z Euler rotations of the joint centre empty. To make this manual process more systematic, starting from the lowest possible Z value (i.e. most flexed viable pose), Z axis rotations were fixed at five or ten

degree increments along the FE range of the elbow, while the joint centre empty (and its meshes) was freely rotated around the X and Y axes simultaneously to capture interaction between these degrees of freedom. Approximately 10 viable poses representing the limits of LAR and ABAD at each FE increment were keyframed, although additional poses were sampled in areas of complex morphology to ensure ROM was sufficiently well captured. Each pose was visually inspected while keyframing, to ensure neither the ulna nor radius meshes intersected the humerus, before shifting to the next Z axis increment and repeating the process until maximum extension was achieved. This resulted in 100–300 keyframed poses for each taxon, depending on its morphology and complexity of DOF interactions, depicting the range of poses achievable by that elbow. The resultant list of keyframed rotation coordinates was then exported as a CSV file (see Supplementary Material 1.2). This process was performed in the same way for each of our nine species, with potential interobserver error minimised by having all articulation, JCS setup and pose sampling performed by a single individual (HLR). This manual pose sampling method, though it employs the same principles, is not as comprehensive or precisely repeatable as the automated method developed by Manafzadeh and Padian (2018). However, we believe that our approach sufficiently characterises joint mobility (Figure 2) and is appropriate in the context of this kind of broad comparative study.

Because our alignment of joint axes along the humeral and ulnar shafts was established by eye, there is some user-dependency in our JCS assignment. Additionally, Manafzadeh and Gatesy (2020) recently demonstrated how distortions intrinsic to the nonlinear mapping of poses into Euler space can affect ROM envelope characteristics and yield different results depending on the JCS used to generate them. To explore the effects of these issues and other model parameters on our results, we performed several sensitivity analyses (see below).

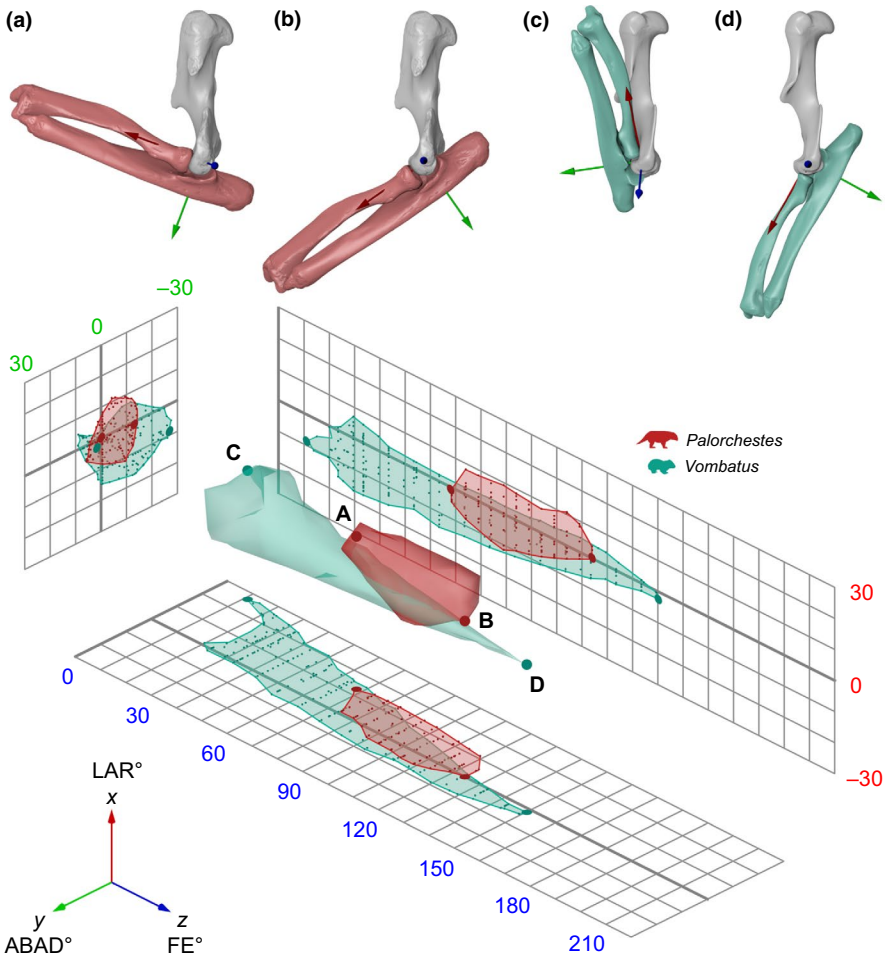

FIGURE 2 Left forelimbs of *Palorchestes* (a, b) and *Vombatus* (c, d) in lateral view demonstrating poses resulting from maximum elbow rotation about the Z axis (flexion–extension, FE) when modelled with a fixed joint centre and three rotational degrees of freedom (XYZ). *Palorchestes* (a) minimum flexion (0°, −12°, 69°) and (b) maximum extension (1°, 1°, 125°); *Vombatus* (c) minimum flexion (−8°, −26°, 12°) and (d) maximum extension (−2°, 3°, 151°). The 3D points representing these minimum (a, c) and maximum (b, d) FE poses are plotted on the ROM map along with the complete ROM envelopes as examples to show how the degrees of freedom interact and how this differs between species. Achieving the full range of FE requires different combinations of abduction–adduction and long-axis rotation in *Palorchestes* compared to *Vombatus*. Points on 2D projections represent all sampled poses to show density of our manual sampling method. Bone models are scaled to same humeral length

2.4 | 3 DOF ROM mapping

Following the approach developed by Haering et al. (2014) and refined by Kambic et al. (2017) and Manafzadeh and Padian (2018), we imported the XYZ rotation coordinates for each taxon into MATLAB R2019b (Mathworks, Natick, MA, USA) and plotted them as points in a Euclidean (non-transformed) angle-angle-angle space. Each point cloud was fitted with an alpha shape, which was then exported as an OBJ file. An alpha radius of 10 was used for all species, set *a priori* as the lowest value that closely encapsulated all points across all species without creating internal holes, thereby generating comparable 3D ROM envelopes. The limits of each volume are defined by the extremes of the keyframed multiaxial rotations, which envelop all other rotation combinations possible for that elbow. As they were generated by rigs using a homologous relative joint centre and JCS, ROM envelopes for all taxa could be visualised on a common set of axes highlighting their relative positions and overlap in space (Figure 2).

2.5 | Quantification of ROM envelopes

As well as mapping the ROM envelopes, we quantified several characteristics to explore patterns in their shape and extent, as measures of ROM similarity between species. Along with volume (in 'cubic degrees') and absolute mobility range along each axis, we also calculated centroids, eigenvalues, eigenvectors and the degree of anisotropy (ratio of the maximum to minimum eigenvalues, that is, where the envelope falls on a spherical-to-prolate spectrum). These calculations were performed using MATLAB functions (supplementary material 2.1), building on previous code published by Allen et al. (2013). Correlations between ROM, volume, anisotropy and body mass were explored using Pearson correlation tests in R Version 3.5.0 (R Core Team, Vienna, Austria).

2.6 | Sensitivity analyses

We tested the sensitivity of our results to variation in three key assumptions of model setup: the spacing of the humeroulnar joint in extinct taxa as determined by upper and lower bounds of body mass estimates, the spacing of the humeroradial joint, and the mediolateral positioning of the fixed joint centre on the distal humerus (detailed in Supplementary Material 1.4).

Additionally, given the manual method used to establish JCSs, we also examined the effects of JCS selection on our results. To do this, we performed a sensitivity analysis where we randomly rotated the JCS axes by (a) up to 10 and (b) up to 20 degrees about each axis (conservatively large margins of error for how other observers may set up the elbow JCS in the context of this study), and re-projected the pose rotation coordinates onto these rotated axes. For each species, we ran 1000 iterations and each time recomputed the alpha shape, its volume, and its anisotropy, to provide a spread of values (Figure 5, Figure S1.4.7). MATLAB code for running this analysis on pose data is available in Supplementary Material 1.4.

2.7 | 6 DOF modelling

Given the characteristically flattened humeroulnar articulation in *Palorchestes*, we investigated whether allowing translational movements substantially increased the available ROM, and whether this brought *Palorchestes* within the same range of values seen in other species. The role of translation in the mammalian humeroulnar joint is poorly understood. Recent *in vivo* fluoroscopic study ('XROMM') on rats (with 'generalised' mammalian elbow morphology) found that it contributed very little to the observed kinematics (Bonnan et al., 2016), but whether this is true for all mammals, especially large ones, is unknown. By exploring translation as well as rotation kinematics (i.e. 6 DOFs), the maximal ROM of this joint could be more thoroughly documented.

We used the same *Palorchestes* rig parameterised for the 3 DOF analysis to explore elbow mobility in 6 DOF. Adding translations to our manual modelling approach necessitated additional qualitative assessment of joint congruence, where poses appearing biologically infeasible or disarticulated, as visually determined by the observer, were excluded. The issues with qualitative assessments of joint disarticulation in 6 DOF ROM models are well recognised (e.g., Jannel et al., 2019), so we attempted to mitigate this by constraining movement via creation of a mesh object representing a physical threshold for joint disarticulation. This was modelled as a separate mesh extruded along the normals of the humeral joint surface, for a distance triple that of the estimated joint space (see Figure S1.3.1). A joint pose was considered feasible if the articular margins of the ulna remained within the space between the humerus and this disarticulation threshold mesh, and bone meshes themselves did not intersect.

In total, 150 poses across the whole mobility range were manually sampled in a fashion similar to the previous approach, where the joint was freely rotated and translated at regular Z axis increments, assessed for bone mesh interpenetration and disarticulation, and keyframed. The resulting pose coordinates were used to generate a ROM envelope.

2.7.1 | Helical axes

In addition to exploring whether allowing translations increased rotation abilities in *Palorchestes*, we also analysed the resulting 6 DOF mobility data using helical axes. As it considers both rotations and translations simultaneously, this approach allows for the relative contributions (importance) of rotation and translation to be examined. Hence, by expressing 6 DOF elbow motion in terms of helical axes, this allowed us to test:

a. to what degree the elbow functioned strictly like a helix (whether along-axis translation occurred with rotations); and
b. the validity of using a fixed joint centre in the 3 DOF analyses, as well as its placement midway between the humeral condyles.

From the 6 DOF poses, we derived a 'mean kinematic trajectory' for the elbow by describing each DOF as a parametric function of rZ (FE), the most variable and likely the most biologically important DOF. We used strictly linear functions for this, to produce the simplest (least assumption-laden) statistical model that encapsulates the overall pattern of how the 6 DOFs vary with one another over the elbow's full mobility. As this mean trajectory is calculated in a Euclidean sense with Euler angles, this model ignores nonlinearities that can occur (cf. Manafzadeh & Gatesy, 2020), and of course does not necessarily indicate the precise kinematic pattern used during any single behaviour in life. Nonetheless, it does capture the essential kinematic pattern – what occurs 'on average'.

We then created 21 evenly spaced nodes along the entire length of this 6 DOF mean kinematic trajectory, spanning the full range of rZ from maximal flexion to maximal extension, and used the above linear equations to derive the 'average' value for the other 5 DOFs at each node (Figure 6a). The 4 × 4 transformation matrices from one 6 DOF node to the next were then computed using the KineMat toolbox for MATLAB (Reinschmidt & Van den Bogert, 1997). From these matrices we calculated the finite helical axis for the transformations between successive nodes (20 in total; as per Spoor & Veldpaus, 1980), as well as the cumulative about-axis rotation and along-axis translation across all 21 nodes. For visualisation purposes, a mean helical axis was computed as the vectorial mean of the 20 individual finite helical axes, and a mean joint centre was computed as the point closest to all 20 finite helical axes in the least squares sense. Comparing the finite helical axes revealed any changes in the location and orientation of the primary joint axis (relative to the humerus) across the range of movement.

As a way of expressing the relative importance of rotation and translation in these helical motions, we computed the overall angle of helical movement using the cumulative translations and rotations across the 21 nodes. Setting the radius of the overall helix equal to the radius of the fitted capitular sphere, we could then calculate the helical or 'thread' angle: a steeper angle indicates a greater translational component, producing a more pronounced helical motion. Hence, comparison of rotations to this 'thread' angle, along with the magnitude of along-axis translation, provided an assessment of the extent to which the elbow of *Palorchestes* behaved as a helical joint. MATLAB code and further details of this analysis are provided in Supplementary Material 3.1.

3 | RESULTS

3.1 | Comparative multiaxial ROM

Mobility ranges are presented in Figure 3. It is worth reiterating that these movements are the maxima in each DOF achieved by allowing non-zero rotations in the other DOFs.

In all species, the largest rotation range was around the Z axis (FE). *Palorchestes* had the lowest FE range (55.6°), while most other species had similar ranges (120.7°–142°). *Zygomaturus* had the highest FE range (174.2°), more than triple the mobility of *Palorchestes*. Reduced olecranon and anconeal processes also contributed to high elbow mobility in *Zygomaturus* around all axes, allowing hyperextension (>180°) and a large amount of lateral rotation (negative LAR). *Melursus* differed from the overall pattern seen in other taxa, with large and approximately equal positive and negative ABAD and LAR ranges. Across other species, ABAD and LAR mobility was not equal in both movement directions. Elbows could abduct more than adduct (ranges were more negative). For these rotations, *Palorchestes* mobility fell within the ranges seen in other species.

Rotation ranges, maxima and minima almost always showed no relationship to body mass. The only exception to this was minimum FE, which had a significant positive correlation to mass (r^2 = 0.49, p = 0.02), meaning smaller species were able to reach slightly more flexed elbow postures (had lower minimum FE) than larger species.

3.2 | 3 DOF ROM map

3D ROM maps illustrating the elbow mobility envelopes of *Palorchestes* relative to the eight other mammals are shown in Figure 4, with 2D projections showing the extent, positions and overlap of these envelopes. Full ROM envelope metrics are available in Supplementary Material 2.2-2.3.

3.2.1 | ROM envelope volume

The smallest ROM envelope volume belonged to *Palorchestes*, with 8395 degrees^3. Volumes for other species ranged from 10,825 degrees^3 in *Orycteropus* to 53,373 degrees^3 in *Melursus*, where their high LAR and ABAD ranges created a volume much greater than other species sampled (Figure 5). This parameter was uncorrelated with body mass (r^2 = 0.01, p = 0.87).

3.2.2 | ROM envelope shape (anisotropy)

The *Palorchestes* envelope, with extremely low FE range but typical LAR and ABAD, appears short and squat in the ROM map, and contrasts with the more elongate shapes of other species (Figure 4). *Palorchestes* had the most 'spherical' ROM envelope, with the lowest anisotropy value (5.27), followed by *Melursus* (9.37). The highest anisotropy value belonged to *Orycteropus* (45.03), which was only slightly more prolate than *Phascolarctos* (43.65) (Figure 5). Anisotropy had no significant correlation with body mass, rotation ranges, maxima/minima or envelope volume.

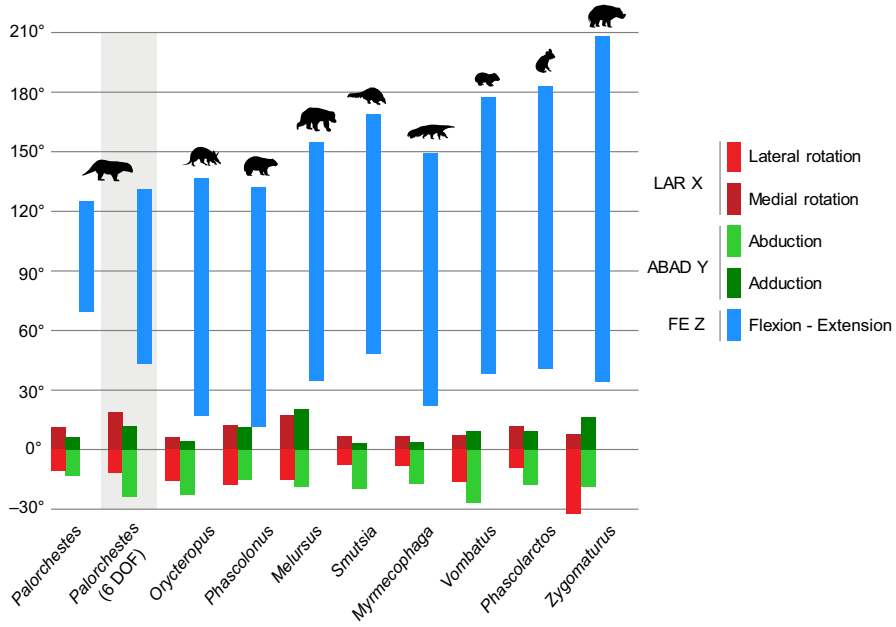

FIGURE 3 Maximum elbow ROM ranges. Multiaxial humeroulnar ROM across our comparative sample of mammals when modelled using a fixed joint centre with three degrees of freedom considered simultaneously. *Palorchestes* was additionally modelled with six degrees of freedom (indicated with grey background), which increased maximum ROM around all axes

3.3 | 3 DOF Sensitivity analyses

Full sensitivity analysis results are available in Supplementary Material 1.4.

3.3.1 | Humeroulnar joint space

Maximum ROM in each axis responded as expected to changes in joint spacing as determined by body size estimates, with maxima increasing and decreasing according to greater or smaller humeroulnar joint spaces, respectively. This also affected the resultant ROM envelope volume in all extinct species. However, the magnitude of this effect varied; the upper mass estimate for *Phascolonus* produced a ROM envelope more than twice the volume of the lower mass prediction, while in *Palorchestes* they varied by less than 40%, with the other species in between. This shows that envelope volume is sensitive to humeroulnar joint space parameterisation, although this is not consistent across morphologies. Anisotropy was relatively insensitive to changes in body mass and humeroulnar joint space, except in *Zygomaturus* where larger joint spacing produced a slightly more spherical shape.

3.3.2 | Radius position

Mobility in LAR and FE was not strongly affected by changes in radius position, where axial rotation and maximal flexion could still be closely approximated by all species tested when the radius was positioned closer to the joint (differences less than 4°). Extension was unaffected except in *Myrmecophaga* and *Smutsia* where the radius collided with the capitulum before full extension was reached. Abduction/adduction was most significantly influenced by radius position, with differences between maximum and minimum radius joint spacing causing differences in ABAD between 13-80%, most notably in *Myrmecophaga*. The volume and shape of envelopes from all species showed similar patterns in sensitivity to humeroradial joint spacing, with most difference occurring when the radius was closer to the humerus. Increasing the joint space made very little difference to the envelopes, indicating the humeroradial joint space assumptions used for modelling these taxa were suitable.

3.3.3 | Joint centre position

Of the parameters tested, our models were most sensitive to changes in joint centre position. It had very little effect on maximum ROM in two of the three species tested, with ranges across all three axes fairly stable. *Myrmecophaga* contrasted with these, where varying the joint centre increased ROM in all cases, most conspicuously in the Y axis where a more lateral joint centre allowed for more than twice the amount of abduction. *Smutsia* was relatively insensitive in envelope volume or shape across models. *Myrmecophaga* was the most sensitive in terms of volume, with both lateral and medial models causing marked volume increase. *Orycteropus* was the most sensitive in terms of envelope shape, generating a very prolate envelope in the lateral model relative to the other species.

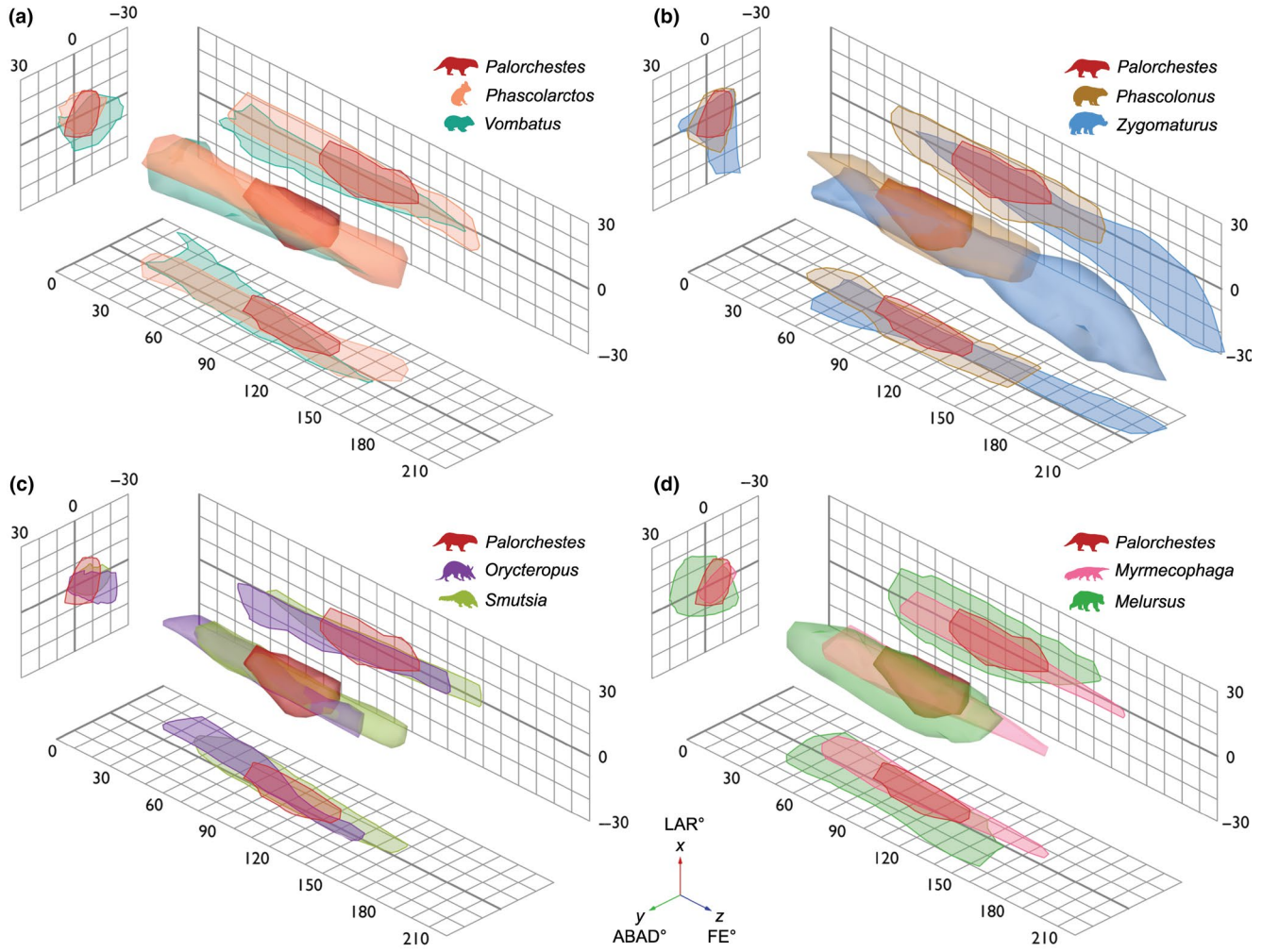

FIGURE 4 Humeroulnar joint 3D ROM maps showing variation in shape and position of ROM envelopes produced by 3 DOF multiaxial elbow rotations in *Palorchestes* and comparative species. *Palorchestes* plotted with other marsupials: (a) extant phylogenetic bracket taxa *Phascolarctos* (koala) and *Vombatus* (common wombat); (b) extinct contemporaneous vombatiform megafauna of similar body size, *Phascolonus* (giant wombat) and *Zygomaturus* (browsing diprotodontid). *Palorchestes* plotted with placental species sharing similar forelimb morphologies which may represent functional analogues: (c) *Orycteropus* (aardvark) and *Smutsia* (giant pangolin); (d) *Myrmecophaga* (giant anteater) and *Melursus* (sloth bear). Views are orthographic and isometric, grids show 2D projections of ROM. Thick grid lines represent zero

3.3.4 | Joint coordinate system

Both envelope volume and anisotropy values were affected by changes to the assigned JCS (Figure 5). When allowing the JCS to vary up to 10 degrees from its original disposition, volume varied by 2–6% and anisotropy by 3–16%, whereas when allowing the JCS to vary up to 20 degrees, volume varied by less than 10% and anisotropy by 10–73% (Figure S1.4.7). This shows anisotropy to be more sensitive to JCS assignment than volume (particularly for more anisotropic mobility spaces), though the general patterns among taxa and their separation from *Palorchestes* were consistent across both analyses.

3.4 | 6 DOF ROM

By modelling translation as well as rotation, the *Palorchestes* elbow achieved greater maximum ROM around all axes compared to the initial 3 DOF analysis, most importantly in FE mobility (Figure 3). However, although *Palorchestes*' FE range increased by 58% from 56° to 88° when modelled with 6 DOF, this range was still substantially lower than the FE ranges seen in other mammals when modelled with 3 DOF. We therefore assume that the other mammals in our sample, if also allowed translational DOFs, would show at least similar if not greater increases in FE ROM, reinforcing this mobility gap between *Palorchestes* and other mammals.

Mobility in ABAD saw the largest difference between 3 and 6 DOF models, increasing by 85% (Figures 3, 4 and 6a). Long-axis rotation also increased between the models, particularly in medial rotation.

When considering interactions between these rotations they appear coupled, as indicated by the skew in the ROM envelope and the node positions of the mean kinematic trajectory (Figure 6a). Extension of the elbow was accompanied by obligate adduction and slight medial rotation, and likewise flexion was coupled with abduction and lateral rotation.

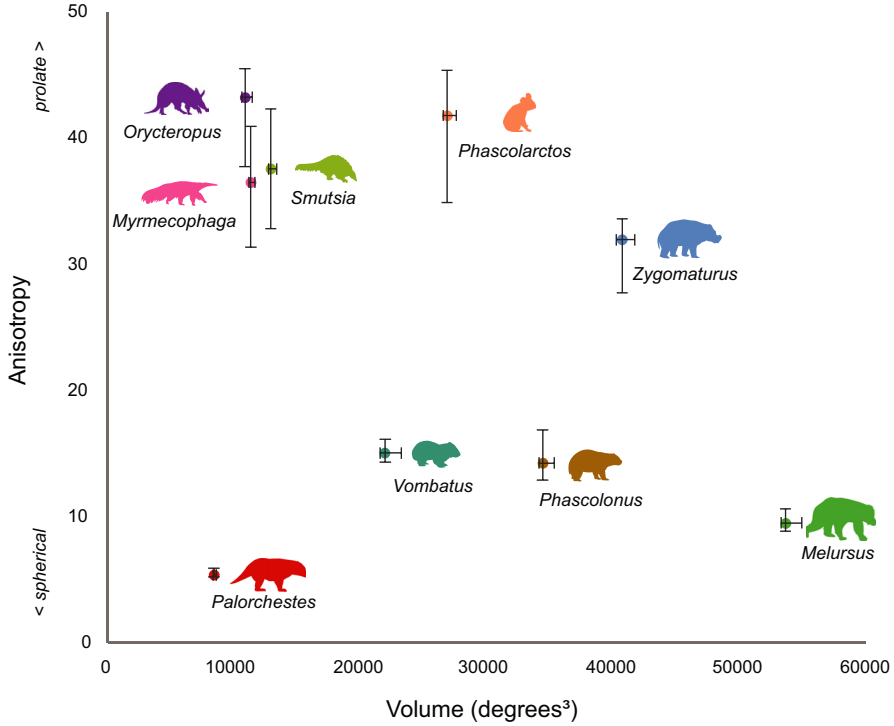

FIGURE 5 Humeroulnar joint ROM envelope quantifications. ROM envelope (alpha shape) volume plotted against anisotropy score (ratio of the maximum to minimum eigenvalues of the alpha shape), showing variation in these envelope characteristics among study species, with *Palorchestes* lowest in both measures. Error bars (max/min) indicate sensitivity of these measures to variation in the manually assigned JCS, where this was randomly varied by up to 10° across 1000 iterations

3.5 | Helical axes

The helical axes analysis showed that translation played only a small role in the kinematics of the *Palorchestes* elbow. Across the whole range of motion, the joint cumulatively underwent approximately 5 mm of translation over 93° of rotation (Figure S3.3). Assuming a helix radius equal to the radius of the sphere fitted to the capitulum, this equates to a 'thread angle' of just over 6°, indicating that elbow movements in *Palorchestes* were only weakly helical at best, with rotational movements largely decoupled from limited translational movements. More importantly, the analysis also revealed that the finite and mean helical axes were markedly skewed with respect to the anatomical axes of the humerus (Figure 6b). This skew changed substantially with increasing elbow extension, where the finite helical axis pivoted in space to follow the contour of the capitulum as the elbow progressed from flexed to extended postures (lateral view in Figure 6b). The mean joint centre calculated from the finite helical axes lay approximately midway between the trochlea and capitulum, supporting our placement of a static joint centre in this position in the 3 DOF analyses.

4 | DISCUSSION

In this study, we set out to quantitatively test previous functional interpretations of the bizarre forelimb anatomy of *Palorchestes*, using 3D ROM mapping of elbow mobility with a comparative dataset of extant and extinct mammals. This multiaxial approach has confirmed that even when degrees of freedom available are maximised, *Palorchestes* has remarkably low elbow mobility compared to other mammals, although this joint may not have been quite as 'fixed' as previously thought (Flannery & Archer, 1985; Richards et al., 2019). Our results highlight that even 'hinge' joints such as the elbow, which have traditionally been assumed to be uniaxial in their movements, can in fact show complex multiaxial rotations in maximal osteological ROM. Additionally, this study confirms that interspecific differences in limb morphology are to an extent reflected as differences in ROM map visualisations, and quantification of these can be a useful comparative tool for understanding and contextualising the functional capabilities of extinct species.

4.1 | *Palorchestes* elbow mobility was lower than other mammals

Our results show that *Palorchestes* had strongly reduced elbow ROM relative to other mammals, indicating a reduced functional capacity. None of our comparison species showed similarities that would indicate direct functional analogy based on these measures of elbow mobility.

Palorchestes elbow mobility was much lower than that of its closest living relatives (Figures 3 and 4a). This difference was expected for the koala, given their arboreal lifestyle and reliance on reaching with the forelimbs during locomotion and feeding (Lee & Carrick, 1989). However, such high elbow mobility was unexpected in the wombat considering their robust forelimbs and fossorial habits, though this may be partly attributable to the absence of soft tissues in these

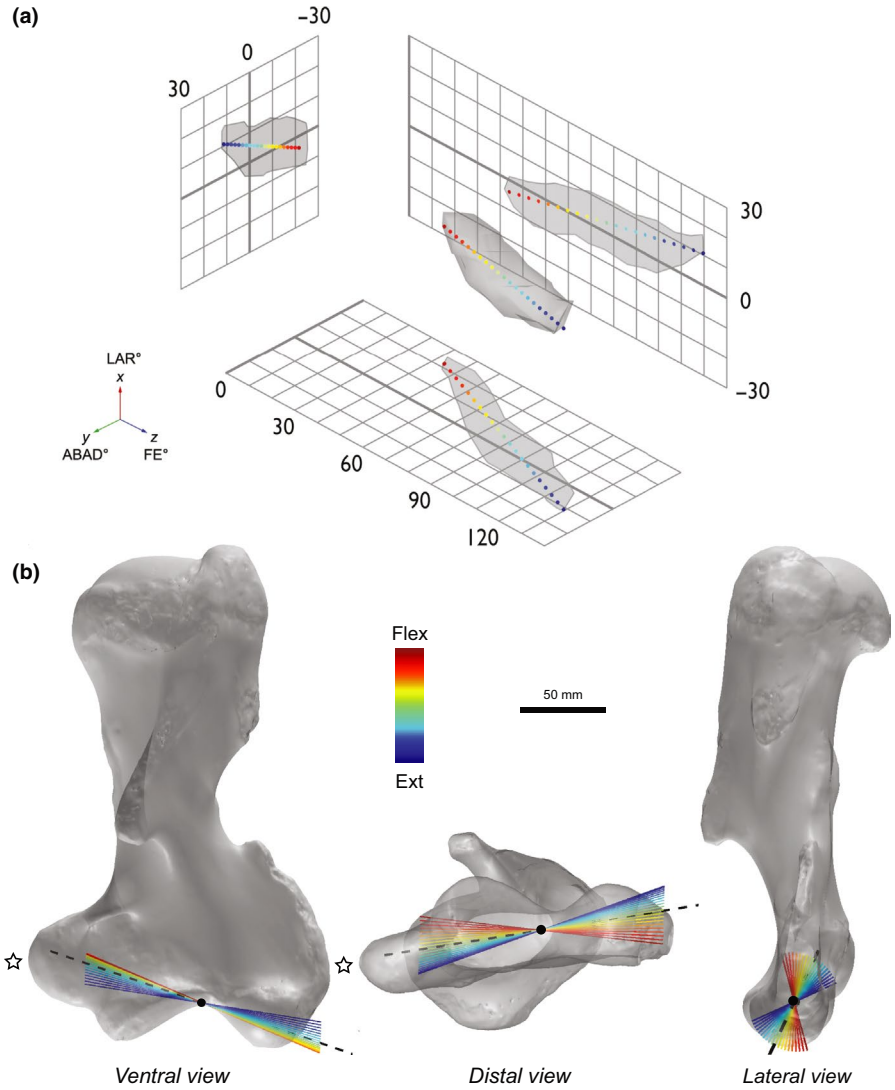

FIGURE 6 Six degrees of freedom elbow movement in *Palorchestes azael*. (a) 3D ROM map showing the ROM envelope produced by 6 DOF multiaxial rotations of the *Palorchestes* elbow, with the 21 nodes of the mean kinematic trajectory plotted (red flexed—blue extended poses). (b) *Palorchestes azael* left humerus with 20 finite helical axes superimposed showing changes in axis orientation over the course of the mean kinematic trajectory (red flexed—blue extended poses) modelled with 6 DOF. Black dashed line indicates the mean helical axis, black dot is the mean joint centre along this axis. Star indicates the medial epicondyle

models (see *Limitations* section below). These results indicate that in the context of joint mobility, the extant phylogenetic bracket does little to inform our understanding of forelimb function in *Palorchestes*.

Elbow mobility in *Palorchestes* also contrasted with its contemporaneous extinct kin of similar body size, particularly *Zygomaturus*. The vast elbow ROM in this species was due to reduced anconeal and strongly deflected olecranon processes, unlike any other taxon in our sample. Such deflected olecranon morphology has been shown to signify habitually extended elbow posture in extant mammals (Fujiwara, 2009) and suggests a more columnar forelimb posture in *Zygomaturus*. This anatomy also allowed extensive (and probably unrealistic) long-axis rotation of the forearm in extended postures (Figures 3 and 4b), suggesting that in this large animal soft tissues played a significant role in joint stabilisation. Despite *Zygomaturus* and *Palorchestes* being the most closely related animals in our analysis, their ROM envelopes differed greatly, with the former having high anisotropy and high volume, in contrast to *Palorchestes*' low anisotropy, low volume shape (Figures 4b and 5). This supports the hypothesis that these related taxa used their forelimbs in substantially different ways (Richards et al., 2019). We suggest that *Zygomaturus* used its forelimbs primarily for locomotion, while *Palorchestes* has morphology strongly adapted for non-locomotor functions, like browsing or scratch digging.

4.2 | *Palorchestes* posture, locomotion, and forelimb use

The exceptionally low FE ROM in *Palorchestes* indicates that this animal maintained an obligate crouched forelimb posture (Figures 3–5). This is highly unusual for large-bodied plantigrade mammals

(Biewener, 2005), and although shared ROM space shows that the similarly sized extinct wombat *Phascolonus* could also adopt such crouched poses, that animal had much more potential elbow movement than *Palorchestes* (Figure 4b). *Palorchestes*' reduced forelimb mobility would have drastically constrained its locomotor and non-locomotor capacity. *In vivo* work on mammals shows that FE rotation in the elbow between stance and swing phases in an average gait cycle in opossums (Jenkins & Weijs, 1979), rats (Bonnan et al., 2016), cats, dogs and horses is between 50° and 60°, and as low as 40° in elephants (Ren et al., 2008). This represents just 30–50% of their maximum osteological ROM, although quadrupedal mammals likely use much more of their potential joint mobility during non-locomotor activities (Ren et al., 2008). This pattern suggests that elbow movement during normal locomotion in *Palorchestes* would have been substantially lower again than the ranges measured here, especially considering the additional restrictions imposed by soft tissues.

Flexed postures are common among small mammals and reduce their effective stride length. In species lacking a clavicle this can be compensated for by a more mobile scapula, shifting the fulcrum of anteroposterior movement dorsally (Fischer, 1994). However, the potential for this kind of scapulothoracic compensation may have been limited in *Palorchestes* due to both increased weight-bearing demands on the shoulder girdle in a ~1000 kg animal and the presence of a bony clavicle (although complete clavicular and scapular material is not yet known for this species). While the presence of a clavicle reduces total anteroposterior excursion of the scapula, it also allows increased abduction—adduction movements to contribute to the stride by propping the shoulder joint away from the body (Jenkins, 1974). This creates a more 'sprawled' posture and gait, contrasting with the parasagittal movements typically thought to characterise larger mammals (Gray, 1968). We predict that to compensate for the obligate crouched forelimb posture and low elbow mobility demonstrated here, *Palorchestes* used an especially abducted shoulder posture, with humeral long-axis rotation assisting the manus to clear the ground during swing phase. Such semi-sprawled posture in *Palorchestes* is corroborated by the strongly enlarged medial epicondyle of their humerus (star in Figure 6b), which is associated with large adductor moments at the elbow characteristic of this kind of locomotion in other tetrapods (Fujiwara & Hutchinson, 2012). An abducted shoulder position would also bring the skewed mean helical axis of the elbow (taken here as a surrogate for the axis of primary movement) perpendicular to the sagittal plane, more effectively orienting the minimal available elbow movement for the execution of the stride (Figure 7). No known fossil trackways are currently attributable to *Palorchestes*, but we speculate such traces may be highly distinctive, reflecting this wide forelimb posture coupled with a comparatively narrow-gauge hindlimb (Richards et al., 2019).

We therefore suggest that *Palorchestes* may have used a flexed, abducted forelimb posture and humeral rotation gait not found among large mammals alive today. This configuration likely increased the effort required of the pectoral girdle musculature to resist collapse due to ground reaction forces. Such a gait could be expected to be slow and energetically inefficient for an animal of this size, compared to the more upright postures and parasagittal locomotion likely in more columnar-limbed extinct vombatiforms like *Zygomaturus*, and seen in forelimbs of living mammalian megafauna such as rhinoceroses, elephants and hippopotamuses (Biewener, 1983). This may have far-reaching consequences for interpretation of *Palorchestes*' palaeoecology: such energetically expensive locomotion potentially limited individual geographic range size, increased predation risk, and reduced the adaptability of the species to any environmental changes that affected spatial availability of food resources. This suggests that *Palorchestes azael* was experiencing strong constraints preventing their forelimb from undergoing the postural shifts associated with optimal locomotion at large body sizes. Most likely this was due to their dependence on the forelimb for food acquisition, a habit which appears to have persisted throughout their lineage given the consistency of specialised palorchestid craniodental and postcranial morphologies since the early Miocene (Richards et al., 2019; Trusler & Sharp, 2016). We suggest this forelimb anatomy may have been used either in scratch digging or, perhaps more likely, bipedal browsing—a functional niche unrepresented among living mammals (Coombs, 1983). This may partly explain the lack of functional similarities recovered in our results, and makes sense given their koala-like claw morphology (Richards et al., 2019). This compromise in locomotor efficiency in favour of other forelimb uses was evidently successful for a time—*Palorchestes azael* is the most common and widely distributed palorchestid, recovered in Middle to Late Pleistocene deposits right across the eastern half of the Australian continent (Davis & Archer, 1997)—until their existence was cut short by the extinctions that decimated Australia's megafauna some 40,000 years ago (Hocknull et al., 2020).

4.3 | Morphofunctional and ecological signal in ROM envelopes

We have shown that some aspects of forelimb posture and function are evident in ROM maps, and that envelope characteristics appear to be largely independent of body size. In addition, some morphological information is reflected in the shapes of ROM envelopes (Figure 3). For example, envelope 'width' (ABAD range) at high FE values is related to the depth and extent of the olecranon fossa on the posterior distal humerus. Shallow fossae in the koala and pangolin allow ABAD of the ulna in extended positions, while deeper fossae in the aardvark and anteater restrict this and create tapered envelopes at high FE values. Most species show widening of the envelope at low FE values, where highly flexed postures provide lower joint congruence and allow more lateral 'play' in the joint, as previously noted in the human elbow (Bottlang et al., 2000). This is particularly interesting in the wombat (Figures 1 and 3a), where the envelope topology in this region appears broad but concave due to collision of the radial shaft with the anteriorly prominent deltopectoral crest, interrupting the ROM in this region. However, such hyper-flexed poses would likely

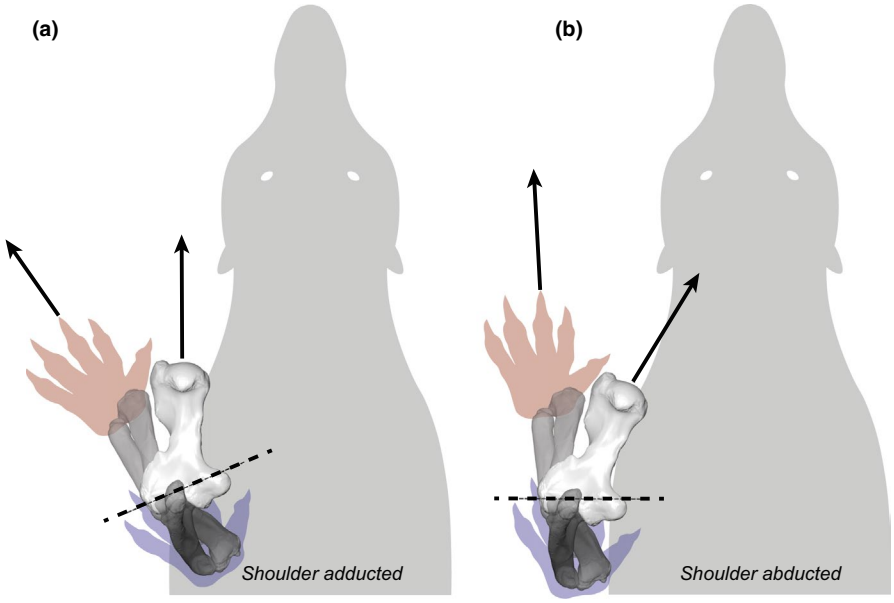

FIGURE 7 Dorsal views of speculative shoulder postures for *Palorchestes*. Long axes of the humerus and manus are indicated with black arrows. Schematic positions of the manus are shown at flexed (red) and extended (blue) positions when the elbow is rotated around the mean helical axis (dashed line). (a) In an adducted shoulder pose with the humerus held along the parasagittal axis as in large extant mammals, the skewed mean helical axis of the elbow causes lateral movement of the manus. (b) By abducting the shoulder, the mean helical axis is perpendicular to the body, and manus movement is aligned with the direction of travel. Actual manus position will also be affected by pronation/supination, scapular movements and soft tissues not considered here

be impossible due to the presence of soft tissues, and require careful interpretation (see *Limitations* below).

Structural differences in the elbow may also be reflected in our ROM maps. *Melursus* has a conspicuously different ROM envelope shape and distribution compared with other species in our analysis (Figure 3d), likely due to their 'derived' carnivoran elbow structure versus the other 'primitive therian' species in our sample (Jenkins, 1973, figure 17, pg. 293). Jenkins hypothesised that this derived structure in carnivorans confers greater stability at the expense of mobility, but our results suggest the opposite. This could be due in part to the reduced definition between the condyles on the distal humerus in *Melursus*, permitting increased mobility without mesh collision in our model, and may indicate increased reliance on soft tissues for joint stabilisation in the bear elbow. Alternatively, the humeroradial joint spacing applied across our models may be less suitable for this type of elbow. Additional *in vivo* data on cartilage thickness and joint spacing across mammal species are required to parameterise these types of models more reliably.

Whether this ROM mapping technique can capture any ecological signal merits further investigation. Some of our results hint that functional similarities among extant species may be interpretable in envelope metrics and shared occupancy of ROM space; for example, the myrmecophagous species in our sample all shared similar volume and anisotropy values (Figure 4). Conversely, the koala did not stand out as having mobility results especially distinct from the other species despite being the only arboreal taxon in our sample. While this study did not set out to demonstrate correspondence of substrate use with elbow mobility, future work incorporating a broader sample of mammals may be able to determine whether patterns can be seen in elbow ROM related to gross differences in substrate use or locomotor mode. If this can be shown, it may provide a tool for palaeobiological inferences in other extinct mammals.

4.4 | ROM envelope quantifications

Prior assessments of 3D ROM map similarity have been descriptive or compared only envelope volume (Kambic et al., 2017; Manafzadeh & Padian, 2018). However, just as 3D multiaxial assessment of ROM is an important expansion from 2D uniaxial methods, in comparative studies it is also useful to assess 3D ROM via more than one metric. For some joints, volume alone may exaggerate or mask meaningful differences in mobility. For example, ROM envelope volume is very sensitive to small absolute changes in elbow LAR and ABAD due to lower ranges along these axes, but FE is probably the most biologically important rotation for this joint. Anisotropy (the ratio of an envelope's maximum to minimum eigenvalues, distinguishing round from elongate shapes) may be a useful supplement to interpretations of envelope volume (but see Limitations below). It appears slightly less affected by differences in model parameterisation (e.g. joint spacing; Supplementary Material 1.4), although shows more sensitivity to variation in JCS selection (Figure 5). This metric could be used to compare ROM envelopes that yield similar volumes, but which may differ in shape, possibly reflecting functional differences.

Supplementing qualitative interpretations, mobility ranges and envelope volumes with this additional metric gives a clearer picture

of variation in ROM envelope shape and maximal joint function, and hopefully provides an additional way to characterise and compare joint mobility in future comparative studies. Anisotropy could also be applied along with volume measures in XROMM work to objectively assess consistency of ROM maps, such as across repeated or contralateral observations of the same individual, intraspecific variability, and interobserver error (cf. Kambic et al., 2017).

5 | LIMITATIONS

5.1 | Soft tissues

Importantly, these models make only a limited attempt to account for soft tissues and must be considered estimates of theoretical maximal osteological ROM (Arnold et al., 2014; Hutson & Hutson, 2015; Manafzadeh & Padian, 2018). This question of soft tissue effects is an ongoing problem in palaeobiological inference of joint mobility (see discussions in Hutson & Hutson, 2015; Pierce et al., 2012). In the present study, we do not know how soft tissues would modify the shape or extent of ROM envelopes observed here, or whether such modification would be uniform around each envelope's perimeter. For example, extensive forelimb muscle bulk, while having little effect on extended postures, would make highly flexed postures such as that of the wombat in Figure 1c biologically implausible (Carpenter & Wilson, 2008). Therefore, low FE values within our envelopes are probably less likely to represent *in vivo* ROM than higher values. Additionally, passive muscle forces, capsular and extracapsular ligaments of the elbow have all been shown to limit LAR and ABAD in cadaveric sheep elbows (Poncery et al., 2019), and while these factors would unquestionably limit ROM modelled here, whether this would affect positive and negative rotations equally is unknown.

However, morphology inherent to the mammalian elbow may make it less sensitive to these assumptions than some other commonly modelled joint complexes. For example, well-developed joint surfaces with less articular cartilage influence probably make mammalian joint 'bone-only' models more reliable than reptile or amphibian models (Bonnan et al., 2013; Brassey et al., 2017; Holliday et al., 2010). In addition, the articulation of the mammalian elbow is fairly congruent and provides bony constraints to movement, in contrast to ball-and-socket joints like the hip, where unconstrained bone-only models can produce unlimited rotations (Carpenter & Wilson, 2008; Pierce et al., 2012). Certainly ligaments, muscles and integument limit elbow mobility in mammals, and progress is being made in modelling these kinds of soft tissues *in silico* (Manafzadeh & Padian, 2018). The extent of this effect could be further investigated in the future via cadaveric XROMM or marker-based motion capture approaches. Such iterative *ex vivo* testing, where soft tissue layers are progressively removed while sampling extreme elbow poses in cadaveric specimens as in recent work on sheep forelimbs (Poncery et al., 2019) and archosaur elbows (Hutson & Hutson, 2012), may prove fruitful both in our understanding of the effects of soft tissues on elbow mobility and in parameterising future biomechanical models of extinct mammals.

5.2 | Spherical coordinates do not map linearly to three-dimensional space

In this study, we introduced anisotropy as a novel metric for quantitatively comparing 3D joint mobility across taxa. While this provided added insight, it nonetheless carries an important caveat. As noted by Manafzadeh and Padian (2018), rotations expressed as Euler angles cannot be linearly mapped to distances along axes in Cartesian coordinate space (Stuelpnagel, 1964), which means that 'cubic degrees' are not directly equivalent everywhere across our ROM maps. However, Manafzadeh and Gatesy (2020) recently showed that the main distortion of Euler space lies along the second rotation axis (Y, ABAD in our case), particularly at absolute values greater than 30 degrees. Because our study focused on the elbow joint, ABAD rotations recovered were fortunately limited relative to other joint complexes such as the hip or shoulder. As our ABAD values for all taxa are well below 30 degrees, our ROM envelopes lie in the least distorted portions of ROM space, reducing the impact of this on our main results and, importantly, our conclusions. While legitimate differences clearly exist between some of the taxa studied here (Figures 4 and 5), we emphasise caution when interpreting the spatial relationships between our ROM envelopes and avoid a literal reading of the quantitative results obtained. Future ROM studies, especially those using this anisotropy metric in quantitative interspecific comparisons, should first apply the cosine corrections proposed by Manafzadeh and Gatesy (2020) prior to visualisations and analyses.

6 | CONCLUSIONS

In this study, we set out to quantitatively investigate elbow mobility in *Palorchestes* and to test how this compared against other mammals sharing structural and perhaps functional affinity with the forelimb of this unusual animal. This was achieved using novel 3D computational and visualisation approaches.

Along its axis of greatest mobility, the *Palorchestes* elbow shows the lowest ROM among the mammals sampled, in both 3 and 6 DOF models. When ROM maps are interpreted along with these conventional maxima and minima, the restricted forelimb kinematics in *Palorchestes* are evident and no species among our sample presents a clear functional analogue. Although prior interpretations of near complete immobility in the elbow joint are not supported (Flannery & Archer, 1985), the *Palorchestes* forelimb was certainly limited to flexed postures highly unusual for a plantigrade mammal of its size. It seems the elbow underwent coupled flexion and abduction, creating a skewed primary axis around which limited movement could occur at this joint. We

suggest *Palorchestes*' locomotion would have been slow and laborious, potentially facilitated by reorienting the humerus to align this off-axis elbow movement with the direction of travel, using a semi-sprawled shoulder posture and humeral rotation movements while walking. The underlying forelimb morphology probably arose as an adaptation to non-locomotor functions like scratch digging or, perhaps more likely, bipedal browsing.

To validate qualitative functional interpretations of the *Palorchestes* forelimb, we have attempted to quantitatively explore the morphology and mobility in its elbow joint. As well as emphasising their distinctiveness among mammals, this work highlights the diversity of kinematic patterns expressed by vombatiform marsupials, and demonstrates a comparative application of ROM mapping approaches.

ETHICS

The koala and wombat material used in this study were obtained as cadavers in collaboration with Museums Victoria under Victorian Department of Environment, Land, Water and Planning Flora and Fauna permit number 10008717.

ACKNOWLEDGEMENTS

The authors thank the museum staff for access to material: Marisa Suvoy, Sara Ketelsen and Eleanor Hoeger (AMNH); Katie Date, Ricky-Lee Erickson, Karen Roberts, and Tim Ziegler (MV); Tammy Gordon (QVMAG); Mary-Anne Binnie (SAM). The authors also thank Mike De Veer (Monash Biomedical Imaging), Alex McDonald, William Parker and Stephen Thompson for scanning support and logistical assistance. HLR thanks Erich Fitzgerald, John Hutchinson, Andréas Jannel, Olga Panagiotopoulou, Peter Trusler and Rod Wells for helpful discussion that assisted inception and completion of this study, and all authors thank editor Anthony Graham and two anonymous reviewers who provided valuable comments that improved this manuscript.

CONFLICTS OF INTEREST

We declare we have no competing interests.

AUTHORS' CONTRIBUTIONS

HLR conceived and designed the study, collected, analysed and interpreted data, and drafted the manuscript. PJB designed the study, developed MATLAB analyses and interpreted data. DPH interpreted data. JWA conceived the study and provided data. ARE conceived and designed the study and interpreted data. All authors critically revised the manuscript and approved its final version.

DATA AVAILABILITY STATEMENT

Code and data are available in the supplementary material and on Figshare (10.26180/13237895). Mesh files are available on Morphosource.org.

ORCID

Hazel L. Richards https://orcid.org/0000-0002-9272-6815

REFERENCES

Allen, V., Bates, K.T., Li, Z. & Hutchinson, J.R. (2013) Linking the evolution of body shape and locomotor biomechanics in bird-line archosaurs. *Nature*, 497, 104–107.

Arnold, P., Fischer, M.S. & Nyakatura, J.A. (2014) Soft tissue influence on ex vivo mobility in the hip of Iguana: Comparison with in vivo movement and its bearing on joint motion of fossil sprawling tetrapods. *Journal of Anatomy*, 225, 31–41.

Besier, T.F., Sturnieks, D.L., Alderson, J.A. & Lloyd, D.G. (2003) Repeatability of gait data using a functional hip joint centre and a mean helical knee axis. *Journal of Biomechanics*, 36, 1159–1168.

Biewener, A.A. (1983) Allometry of quadrupedal locomotion: The scaling of duty factor, bone curvature and limb orientation to body size. *Journal of Experimental Biology*, 105, 147–171.

Biewener, A.A. (2005) Biomechanical consequences of scaling. *Journal of Experimental Biology*, 208, 1665.

Bishop, P.J., Cuff, A.R. & Hutchinson, J.R. (2020) How to build a dinosaur: Musculoskeletal modeling and simulation of locomotor biomechanics in extinct animals. *Paleobiology*, 1–38.

Black, K.H., Archer, M., Hand, S.J. & Godthelp, H. (2012) The rise of Australian marsupials: A synopsis of biostratigraphic, phylogenetic, palaeoecologic and palaeobiogeographic understanding. In: Talent, J.A. (Ed.) *Earth and life*. The Netherlands: Springer.

Bonnan, M., Shulman, J., Varadharajan, R., Gilbert, C., Wilkes, M., Horner, A. & et al. (2016) Forelimb kinematics of rats using XROMM, with implications for small eutherians and their fossil relatives. *PLoS One*, 11, e0149377.

Bonnan, M.F., Wilhite, D.R., Masters, S.L., Yates, A.M., Gardner, C.K. & Aguiar, A. (2013) What lies beneath: Sub-articular long bone shape scaling in eutherian mammals and saurischian dinosaurs suggests different locomotor adaptations for gigantism. *PLoS One*, 8, e75216.

Bottlang, M., Madey, S.M., Steyers, C.M., Marsh, J.L. & Brown, T.D. (2000) Assessment of elbow joint kinematics in passive motion by electromagnetic motion tracking. *Journal of Orthopaedic Research*, 18, 195–202.

Brainerd, E.L., Baier, D.B., Gatesy, S.M., Hedrick, T.L., Metzger, K.A., Gilbert, S.L. & et al. (2010) X-ray reconstruction of moving morphology (XROMM): Precision, accuracy and applications in comparative biomechanics research. *Journal of Experimental Zoology Part A: Ecological Genetics and Physiology*, 313, 262–279.

Brassey, C.A., Maidment, S.C.R. & Barrett, P.M. (2017) Muscle moment arm analyses applied to vertebrate paleontology: A case study using Stegosaurus stenops Marsh, 1887. *Journal of Vertebrate Paleontology*, 37, e1361432.

Carpenter, K. & Wilson, Y. (2008) A new species of Camptosaurus (Ornithopoda: Dinosauria) from the Morrison Formation (Upper Jurassic) of Dinosaur National Monument, Utah, and a biomechanical analysis of its forelimb. *Annals of Carnegie Museum*, 76, 227–263.

Chèze, L., Fregly, B. & Dimnet, J. (1998) Determination of joint functional axes from noisy marker data using the finite helical axis. *Human Movement Science*, 17, 1–15.

Coombs, M.C. (1983) Large mammalian clawed herbivores: A comparative study. *Transactions of the American Philosophical Society*, 73, 1–96.

Davis, A. & Archer, M. (1997) *Palorchestes azael* (Mammalia, Palorchestidae) from the late Pleistocene Terrace Site Local Fauna, Riversleigh, northwestern Queensland. *Memoirs of the Queensland Museum*, 41, 315–320.

Ehrig, R.M. & Heller, M.O. (2019) On intrinsic equivalences of the finite helical axis, the instantaneous helical axis, and the SARA approach. A mathematical perspective. *Journal of Biomechanics*, 84, 4–10.

Fischer, M.S. (1994) Crouched posture and high fulcrum, a principle in the locomotion of small mammals: The example of the rock hyrax

(Procavia capensis) (Mammalia: Hyracoidea). *Journal of Human Evolution*, 26, 501–524.

Flannery, T.F. & Archer, M. (1985) *Palorchestes*: Large and small palorchestids. In: Rich, P.V., Van Tets, G.F. and Knight, F. (Eds.) *Kadimakara: Extinct vertebrates of Australia*. Melbourne, Victoria: Pioneer Design Studio.

Fujiwara, S. (2009) Olecranon orientation as an indicator of elbow joint angle in the stance phase, and estimation of forelimb posture in extinct quadruped animals. *Journal of Morphology*, 270, 1107–1121.

Fujiwara, S.-I. & Hutchinson, J.R. (2012) Elbow joint adductor moment arm as an indicator of forelimb posture in extinct quadrupedal tetrapods. *Proceedings of the Royal Society B: Biological Sciences*, 279, 2561–2570.

Grand, T.I. & Barboza, P.S. (2001) Anatomy and development of the koala, Phascolarctos cinereus: An evolutionary perspective on the superfamily Vombatoidea. *Anatomy and Embryology*, 203, 211–223.

Gray, J. (1968) *Animal locomotion*. New York: Norton.

Grood, E.S. & Suntay, W.J. (1983) A Joint Coordinate System for the Clinical Description of Three-Dimensional Motions: Application to the Knee. *Journal of Biomechanical Engineering*, 105(2), 136–144. https://doi.org/10.1115/1.3138397

Haering, D., Raison, M. & Begon, M. (2014) Measurement and description of three-dimensional shoulder range of motion with degrees of freedom interactions. *Journal of Biomechanical Engineering*, 136.

Haines, R.W. (1946) A revision of the movements of the forearm in tetrapods. *Journal of Anatomy*, 80, 1.

Hocknull, S.A., Lewis, R., Arnold, L.J., Pietsch, T., Joannes-Boyau, R., Price, G.J. et al. (2020) Extinction of eastern Sahul megafauna coincides with sustained environmental deterioration. *Nature Communications*, 11, 1–14.

Holliday, C.M., Ridgely, R.C., Sedlmayr, J.C. & Witmer, L.M. (2010) Cartilaginous epiphyses in extant archosaurs and their implications for reconstructing limb function in dinosaurs. *PLoS One*, 5, e13120.

Hutchinson, J.R., Anderson, F.C., Blemker, S.S. & Delp, S.L. (2005) Analysis of hindlimb muscle moment arms in Tyrannosaurus rex using a three-dimensional musculoskeletal computer model: Implications for stance, gait, and speed. *Paleobiology*, 31, 676–701.

Hutson, J.D. & Hutson, K.N. (2012) A test of the validity of range of motion studies of fossil archosaur elbow mobility using repeated-measures analysis and the extant phylogenetic bracket. *The Journal of Experimental Biology*, 215, 2030–2038.

Hutson, J. & Hutson, K. (2015) Inferring the prevalence and function of finger hyperextension in Archosauria from finger-joint range of motion in the American alligator. *Journal of Zoology*, 296, 189–199.

Jannel, A., Nair, J.P., Panagiotopoulou, O., Romilio, A. & Salisbury, S.W. (2019) "Keep your feet on the ground": Simulated range of motion and hind foot posture of the Middle Jurassic sauropod Rhoetosaurus brownei and its implications for sauropod biology. *Journal of Morphology*, 280, 849–878.

Jenkins, F.A. (1973) The functional anatomy and evolution of the mammalian humero-ulnar articulation. *Developmental Dynamics*, 137, 281–297.

Jenkins, F.A. (1974) The movement of the shoulder in claviculate and aclaviculate mammals. *Journal of Morphology*, 144, 71–83.

Jenkins, P.A. & Weijs, W.A. (1979) The functional anatomy of the shoulder in the Virginia opossum (Didelphis virginiana). *Journal of Zoology*, 188, 379–410.

Kaashoek, M., Hobbs, S.J., Clayton, H.M., Aerts, P. & Nauwelaerts, S. (2019) Orientation and location of the finite helical axis of the equine forelimb joints. *Journal of Morphology*, 280, 712–721.

Kambic, R.E., Roberts, T.J. & Gatesy, S.M. (2014) Long-axis rotation: A missing degree of freedom in avian bipedal locomotion. *The Journal of Experimental Biology*, 217, 2770–2782.

Kambic, R.E., Roberts, T.J. & Gatesy, S.M. (2017) 3-D range of motion envelopes reveal interacting degrees of freedom in avian hind limb joints. *Journal of Anatomy*, 231, 906–920.

Lai, P.H., Biewener, A.A. & Pierce, S.E. (2018) Three-dimensional mobility and muscle attachments in the pectoral limb of the Triassic cynodont Massetognathus pascuali (Romer, 1967). *Journal of Anatomy*, 232, 383–406.

Lee, A.K. & Carrick, F.N. (1989) Phascolarctidae. In: Walton, D.W. and Richardson, B.J. (Eds.) *Fauna of Australia*. Canberra: AGPS.

Mackness, B.S. (2008) Reconstructing *Palorchestes* (Marsupialia: Palorchestidae) – From giant kangaroo to marsupial 'tapir'. *Proceedings of the Linnean Society of New South Wales*, 130, 21–36.

Mallison, H. (2010) The digital Plateosaurus II: An assessment of the range of motion of the limbs and vertebral column and of previous reconstructions using a digital skeletal mount. *Acta Palaeontologica Polonica*, 55, 433–458.

Manafzadeh, A.R. & Gatesy, S.M. (2020) A coordinate-system-independent method for comparing joint rotational mobilities. *The Journal of Experimental Biology*, jeb.227108.

Manafzadeh, A.R. & Padian, K. (2018) ROM mapping of ligamentous constraints on avian hip mobility: Implications for extinct ornithodirans. *Proceedings of the Royal Society B: Biological Sciences*, 285, 20180727.

McDonald, H., Vizcaíno, S. & Bargo, M.S. (2008) Skeletal anatomy and the fossil history of the Vermilingua. In: Vizcaíno, S. and Loughry, W. (Eds.) *The biology of the Xenarthra*.

Nyakatura, J.A., Allen, V.R., Lauströer, J., Andikfar, A., Danczak, M., Ullrich, H.-J. et al. (2015) A three-dimensional skeletal reconstruction of the stem amniote *Orobates pabsti* (Diadectidae): Analyses of body mass, centre of mass position, and joint mobility. *PLoS One*, 10, e0137284.

Nyakatura, J.A., Melo, K., Horvat, T., Karakasiliotis, K., Allen, V.R., Andikfar, A. et al. (2019) Reverse-engineering the locomotion of a stem amniote. *Nature*, 565, 351–355.

Owen, R. (1873) On the Fossil Mammals of Australia. Family Macropodidae. Genera *Macropus*, *Pachysiagon*, *Leptosiagon*, *Procoptodon*, and *Palorchestes* - Part IX. *Proceedings of the Royal Society of London*, pp. 386–387.

Pierce, S.E., Clack, J.A. & Hutchinson, J.R. (2012) Three-dimensional limb joint mobility in the early tetrapod Ichthyostega. *Nature*, 486, 523–527.

Poncery, B., Arroyave-Tobón, S., Picault, E. & Linares, J.-M. (2019) Effects of realistic sheep elbow kinematics in inverse dynamic simulation. *PLoS One*, 14, e0213100.

Puttaraju, R.C. (2015) Morphological studies of fore limb bones in sloth bear (*Melursus ursinus*). MSc, Karnataka Veterinary Animal And Fisheries Sciences University, Bidar.

Regnault, S. & Pierce, S.E. (2018) Pectoral girdle and forelimb musculoskeletal function in the echidna (Tachyglossus aculeatus): insights into mammalian locomotor evolution. *Royal Society Open Science*, 5, 181400.

Reinschmidt, C. & Van den Bogert, T. (1997) *KineMat: A MATLAB toolbox for three-dimensional kinematic analyses*. Calgary, Canada: Human Performance Laboratory, The University of Calgary.

Ren, L., Butler, M., Miller, C., Paxton, H., Schwerda, D., Fischer, M.S. & et al. (2008) The movements of limb segments and joints during locomotion in African and Asian elephants. *Journal of Experimental Biology*, 211, 2735–2751.

Richards, H.L., Wells, R.T., Evans, A.R., Fitzgerald, E.M. & Adams, J.W. (2019) The extraordinary osteology and functional morphology of the limbs in Palorchestidae, a family of strange extinct marsupial giants. *PLoS One*, 14, e0221824.

Roberts, R.G., Flannery, T.F., Ayliffe, L.K., Yoshida, H., Olley, J.M., Prideaux, G.J. et al. (2001) New ages for the last Australian megafauna: Continent-wide extinction about 46,000 years ago. *Science*, 292, 1888–1892.

Scott, G.G. & Richardson, K.C. (1988) Appendicular osteological differences between *Lasiorhinus latifrons* Owen 1845 and *Vombatus*

ursinus Shaw 1800 (Marsupialia: Vombatidae). *Records of the South Australian Museum*, 22, 95–102.

Scott, H.H. (1915) *A monograph of Nototherium Tasmanicum: Genus Owen: Sp. nov*. Hobart, Tasmania, J. Vail, Government Printer..

Senter, P. & Robins, J.H. (2005) Range of motion in the forelimb of the theropod dinosaur Acrocanthosaurus atokensis, and implications for predatory behaviour. *Journal of Zoology*, 266, 307–318.

Shean, D.A. (2007) Geochronology, taxonomy and morphology of select fossils of the Buchan Caves, south-eastern Australia. MSc thesis, Monash University. https://doi.org/10.4225/03/5a03c3e03e20d

Spoor, C. & Veldpaus, F. (1980) Rigid body motion calculated from spatial co-ordinates of markers. *Journal of Biomechanics*, 13, 391–393.

Steyn, C., Soley, J.T. & Crole, M.R. (2018) Osteology and radiological anatomy of the thoracic limbs of Temminck's ground pangolin (Smutsia temminckii). *The Anatomical Record*, 301, 624–635.

Stirling, E. (1913) On the identity of *Phascolomys* (*Phascolonus*) *gigas*, Owen, and *Sceparnodon ramsayi*, Owen: A description of some of its remains. *Memoirs of the Royal Society South Australia*, 1, 127–178.

Stokdijk, M., Meskers, C., Veeger, H., De Boer, Y. & Rozing, P. (1999) Determination of the optimal elbow axis for evaluation of placement of prostheses. *Clinical Biomechanics*, 14, 177–184.

Stuelpnagel, J. (1964) On the parametrization of the three-dimensional rotation group. *SIAM Review*, 6, 422–430.

Thewissen, J. & Badoux, D. (1986) The descriptive and functional myology of the fore-limb of the aardvark (Orycteropus afer, Pallas 1766). *Anatomischer Anzeiger*, 162, 109–123.

Trusler, P.W. & Sharp, A.C. (2016) Description of new cranial material of *Propalorchestes* (Marsupialia: Palorchestidae) from the middle Miocene camfield beds, Northern Territory, Australia. *Memoirs of Museum Victoria*, 74, 291–324.

Willing, R.T., Nishiwaki, M., Johnson, J.A., King, G.J.W. & Athwal, G.S. (2014) Evaluation of a computational model to predict elbow range of motion. *Computer Aided Surgery*, 19, 57–63.

Witmer, L.M. (1995) The extant phylogenetic bracket and the importance of reconstructing soft tissues in fossils. In: Thomason, J. (Ed.) *Functional morphology in vvertebrate paleontology*. Cambridge University Press.

Woltring, H., Huiskes, R., De Lange, A. & Veldpaus, F. (1985) Finite centroid and helical axis estimation from noisy landmark measurements in the study of human joint kinematics. *Journal of biomechanics*, 18, 379–389.

SUPPORTING INFORMATION

Additional supporting information may be found online in the Supporting Information section.

How to cite this article: Richards HL, Bishop PJ, Hocking DP, Adams JW, Evans AR. Low elbow mobility indicates unique forelimb posture and function in a giant extinct marsupial. *J Anat*. 2021;238:1425–1441. https://doi.org/10.1111/joa.13389